

Targeted Nonlinear Adversarial Perturbations in Images and Videos

Roberto Rey-de-Castro
Princeton University
rrey@princeton.edu

Herschel Rabitz
Princeton University
hrabitz@princeton.edu

Abstract

We introduce a method for learning adversarial perturbations targeted to individual images or videos. The learned perturbations are found to be sparse while at the same time containing a high level of feature detail. Thus, the extracted perturbations allow a form of object or action recognition and provide insights into what features the studied deep neural network models consider important when reaching their classification decisions. From an adversarial point of view, the sparse perturbations successfully confused the models into misclassifying, although the perturbed samples still belonged to the same original class by visual examination. This is discussed in terms of a prospective data augmentation scheme. The sparse yet high-quality perturbations may also be leveraged for image or video compression.

1 Introduction

A longstanding goal in the field of artificial intelligence (AI) is the realization of artificial general intelligence (AGI) [1] which would enable a computer to perform any intellectual task accessible to a human brain. One of the many challenges to be overcome before achieving AGI is the development of computer models with enough capacity to process the highly complex phenomena customarily managed by a human brain. Another outstanding challenge is finding practical ways for comprehensively conveying to algorithms what a human understands from each data sample. While full AGI has proven elusive, there has been considerable recent progress in enabling machines to emulate humans in specialized tasks. Notably, advances in image classification [2, 3, 4], language translation [5], self-driving car technology [6], cancer detection [7], etc. often achieve near- or sometimes super-human performance. This recent progress has been enabled by the application of deep neural network architectures [8] that allow

a machine to learn complex abstract representations. A question relevant to both AGI and specialized AI is to what extent current algorithms capture the relevant representations or features that enable human reasoning. Answering this question requires, as a first step, translating into human terms what a computer model has considered essential in reaching its decisions [9]. One method for extracting this type of information consists of introducing perturbations into the inputs of a computer model and then inspecting the model responses [10, 11, 12, 13]. Relevant perturbations that obscure features important to the model will have a large effect on the model outputs. Here we report on a nonlinear perturbation approach capable of learning optimal perturbations that drastically change the original model output while keeping the input as close as possible to the original one. The perturbation method is applied to image and video classification models. Importantly, the perturbations are generated by deep convolutional neural networks (convnets) able to learn complex (yet minimalistic) perturbations targeted to each particular sample. In implementing the technique we confirmed the results of previous research in that while the studied models do consider some features that are indeed relevant to humans [14, 15, 11, 10], the models are also easily confused by the introduction of seemingly subtle perturbations [12, 13, 16, 17, 18, 19] that do not change the image or video classification from a human’s perspective. To mitigate the latter issue we consider enhancements to data augmentation procedures as suggested by Szegedy et. al. [12]. The process of data augmentation can be greatly improved through the addition of perturbations known to drastically affect the performance of a model (to be improved through re-training) but that do not change the classification of an object from the point of view of a human assessment [12, 13, 20]. Enhancing data augmentation through perturbations provides with a way of “telling” the model (to be re-trained) what a human understands but was not possible to convey to it during

the first round of model training. Furthermore, since the learned perturbations tend to expose the most salient features of an object or action in question, the learned perturbations can be applied to perform object or action detection in images or videos. This extracted information also opens a window into what the model considered important in reaching its decisions in terms understandable by humans. Finally, the observed sparsity of the most relevant perturbations may be leveraged for a novel form of image and video compression and approximate reconstruction.

Our specific contributions may be summarized as follows:

1. We introduce a method for learning adversarial perturbations targeted to a specific sample image or video.
2. We introduce a form of object or action detection/explanation of model outcomes based on the outstanding perturbations.
3. We propose an iterative model training procedure relying on image or video data augmentation to be repeated until a measurable score reaches certain values.
4. We propose a method for image or video compression and approximate reconstruction.

2 Related work

2.1 Perturbations of images

Soon after the release of the first widely successful deep learning models for image classification, perturbation schemes were proposed for understanding them [14] or for exposing some of their shortcomings through the generation of adversarial perturbations that confuse the models into misclassifying [12]. These two areas of study using perturbation methods have seen considerable progress over the years.

Following the seminal work of Szegedy et. al. [12] on adversarial perturbations, the linear nature of convolutional layers (before activation functions) was exploited for the rapid generation of adversarial examples [13]. The existence of (untainted) real-world images that also cause deep learning models to misclassify has also been reported [16]. These and other findings triggered a wave of introspection resulting on a series of comprehensive studies such as an evaluation of the robustness of neural networks [21, 22], model generalization assessments [23, 22], and a proof of the existence of universal adversarial perturbations that can be applied to any image [19]. An impressive

consequence of the latter result may be found in the work of Baluja and Fisher [18] who were able to train adversarial models on a full dataset of images with the explicit goal of confusing a target model into believing that all of the samples belong to an arbitrarily chosen class.

The intrinsic complexity of deep neural networks has led many researchers into attempting to understand model decisions through perturbative tests. Understanding the outcomes of deep learning models has attracted much attention due to its potential for accelerating the field’s progress and rate of adoption [9] and due to recent changes in regulatory requirements [24]. Perturbational approaches for understanding the outcomes of image classification models include greedy search approaches in which parts of the image are occluded [14] or grayed out [15] until it is misclassified. In these cases the result is a saliency map that indicates how strongly the pixels in the image correlate with the output class score. Thus, the most intense regions in each map are considered to be related to image features important in the corresponding model decision. It is also possible to construct a simpler local model around a given image (in the space of inputs) by sampling around it through the introduction of small perturbations [10]. The sampled points are often fitted by a linear regressor with L1 regularization (e.g., Lasso) which enables an identification of the image’s most salient features from the model’s perspective. Finer image features that are relevant to the model’s decision can be exposed by iteratively optimizing the values of a multiplicative gray scale mask [11]. The mask values determine the degree of blurring in the perturbed image and noise is introduced to mitigate optimization artifacts.

To different degrees, most of the perturbation schemes mentioned above are able to perform a form of object localization by extracting a mask (often defined as the difference between the perturbed and original images) with most intense values around the object in question.

2.2 Perturbations of videos

The only previous work that we are aware of regarding perturbations of video samples for the study of deep neural network models was recently published by Wei et. al. [25]. In this study, video pixels are modified to reduce the class score assigned to the original video while attempting to keep the perturbed video as close as possible to the original one. Modifications to the original video are confined to a few video frames by the use in the temporal direction of

a $L1$ norm penalty during the optimization and by the introduction of a mask that explicitly prevents modifications to some frames. The authors were able to produce sparse adversarial perturbations that considerably reduced the original score assigned by the model.

2.3 Perturbative data augmentation

Due to the large number of parameters present in deep neural networks, generally a very large number of training samples is necessary to prevent overfitting. This fact was recognized early on in the development of modern convnet architectures [2] and prompted the development of data augmentation techniques. Early image data augmentation was achieved by shifting, rotating, cropping, and flipping the images [2, 26]. More recently, other heuristics have been used for data augmentation such as color casting, vignetting and lens distortion [27] leading to the training of more robust image classification models. In general, any transformation that does not change the class of a sample can be exploited for data augmentation. Thus, adversarial image perturbations generated by a learned perturbative mask [12, 13, 20] or through the training of generative adversarial networks (GANs) [28] have been proposed for data augmentation. GANs have been successfully applied to the augmentation of biomedical images [29] field in which the number of available samples is limited.

2.4 Video and image reconstruction

Deep neural networks of various architectures have been applied to image and video reconstruction tasks. These include image denoising [30, 31, 32, 33, 34, 35], image super-resolution [36, 37], video super-resolution [38], and video compressive sensing [39, 40].

3 Learned perturbations

A procedure for learning minimalistic input perturbations that drastically modify the outputs of image or video classification models is described next. Assume that there is a trained model M that transforms an input array \mathbf{X} into an output array \mathbf{y} , i.e.,

$$\mathbf{y} = M(\mathbf{X})$$

The elements of output array \mathbf{y} indicate the probabilities of associated classes. Let us denote by k_1, \dots, k_5 the indices corresponding to the largest 5 output values y_{k_1}, \dots, y_{k_5} . The goal here is to obtain a per-

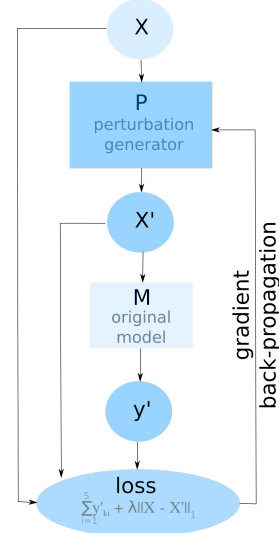


Figure 1: Block diagram illustration of the optimum perturbation search procedure. The input \mathbf{x} and the model M are shaded to indicate that their values or parameters are kept constant during loss minimization.

turbed input \mathbf{X}' with associated output $\mathbf{y}' = M(\mathbf{X}')$ such that:

1. $\sum_{i=1}^5 |y'_{k_i}| \ll 1$ (i.e., the perturbed scores for the originally top 5 classes are minimized).
2. $\|\mathbf{X} - \mathbf{X}'\| \ll 1$ (i.e., the perturbed input is as close as possible to the original input).

In order to accomplish both aims above another model P is used to produce the perturbed inputs $\mathbf{X}' = P(\mathbf{X})$ and the parameters of P are iteratively modified to approach both conditions. Figure 1 illustrates the adaptive procedure used to optimize the parameters of model P . In mathematical form, the optimum parameters of model P are the approximate result of minimizing a loss function expressing the two conditions above, i.e.,

$$\min_P \left[\sum_{i=1}^5 M(P(\mathbf{X})_{k_i}) + \lambda \|\mathbf{X} - P(\mathbf{X})\|_1 \right] \quad (1)$$

where $\|\mathbf{X}\|_1$ denotes the $L1$ norm of tensor \mathbf{X} and λ is a constant for balancing the two terms in the loss. By minimizing the top 5 original outputs, as opposed to only a single top class, the algorithm above ensures that all the important features present in the input are considered (e.g., otherwise small perturbations could be inserted to simply transform a dog image from one breed of dog to another similar one).

This is particularly important in cases when the top class score is not outstanding.

It is also possible to attempt maximizing an specified class with index m , in this case the parameters of model P are modified such that

$$\min_P \left[\sum_{i=1}^5 (1 - M(P(\mathbf{X})_m) + \lambda \|\mathbf{X} - P(\mathbf{X})\|_1) \right] \quad (2)$$

Section 4 shows the results of implementations of the perturbation procedure to image and video models.

4 Experiments

4.1 Implementation details

There is wide versatility in the choice of the perturbation generator P . In general, a suitable choice for P is any model architecture able to produce meaningful perturbations on the input. In the present case P was taken as a convnet for generating perturbations on both images and videos. The particular convnet architecture used here consisted of three blocks each containing three convolutional layers. Each block was followed by a rectified linear (relu) layer. All convolutional layers had 3 channels (corresponding to the three basic colors) and their kernels were taken as (3,3) or (3,3,3) for the analysis of image or video models, respectively. The convolutional layer padding was chosen so as to preserve the original input dimensions. The loss given by eq. (1) or eq. (2) was iteratively reduced by a gradient descent algorithm (Adam optimizer [41]) that modified all the convolutional weights (filters) and biases of the perturbation generator P . The convolutional layer weights and biases were initialized such that tensors passed through them unmodified during the first epoch.

The core of the code was written using the pytorch deep learning framework [42]. The analyzed image classification model (VGG19 [3]) along with its pre-trained weights were automatically downloaded through pytorch’s wrapper to the torchvision package [43]. The studied video classification model (I3D [44]) with its pre-trained weights were downloaded from a github repository [45].

Image and video manipulations made use of the scikit-image and scikit-video packages, respectively. Image samples were downloaded from google images. Video samples corresponding to randomly drawn rows from the kinetics dataset [46] were downloaded from their corresponding YouTube urls.

The experiments were run on a NVIDIA Titan X GPU. All the codes and data mentioned in this paper are publicly available on github [47].

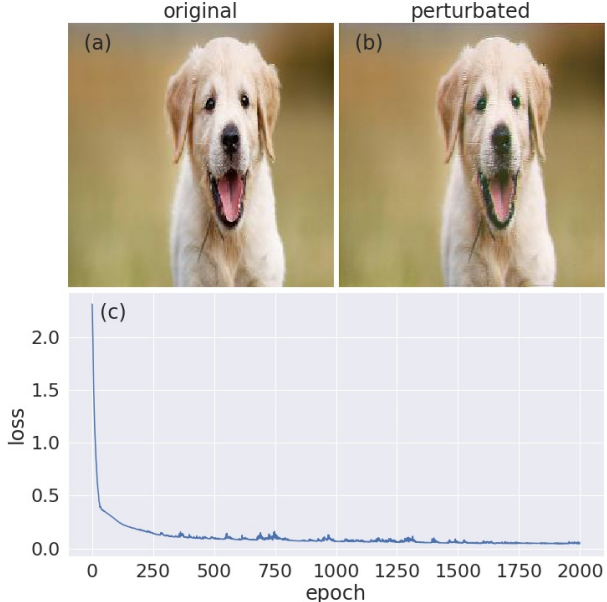


Figure 2: Results of the perturbative procedure applied to the image classification model VGG19. (a) original image sample. (b) The optimum perturbed image that minimized the loss by simultaneously minimizing the top 5 VGG19 scores in the original image while attempting to keep the perturbed image as close as possible to the original one. (c) Loss history through the learning iterations (epochs).

4.2 Perturbating images (VGG19)

The broadly used VGG19 model for image classification [3] was chosen as a first target model for the perturbative procedure described in Sec. 3. Figure 2 shows the results on one of the considered image samples. The original sample (fig. 2(a)) was first resized to 224x224 and scaled as required for the inputs of VGG19 [3] and then fed to the iterative algorithm depicted in fig. 1. The loss function in eq. 1 was then minimized. Parts (b) and (c) of fig. 2 show the optimum perturbed image that minimized the loss and the loss history through the learning iterations (epochs), respectively. The dog in the perturbed image has a slightly lower contrast than in the original one. Nevertheless, both images are very different from VGG19’s point of view. The top 5 scoring image classes, as evaluated by VGG19, for the original and perturbed images are given as “sample 1” entries in table 1. The relatively mild inserted perturbations turned the dominant VGG19 class from “kuvasz” (a dog breed) to “African grey” (a parrot).

Optimal learned perturbations were extracted from a total of six samples downloaded from google images. The results are shown in fig. 3. The first, second,

and third columns of images correspond to the original, perturbed, and the difference between original and perturbed images, respectively. Since the jpeg image format only accepts image data values in the range from 0 to 1, the absolute value of the difference between the original and perturbed images were taken for constructing the difference images. In all cases the VGG19 scores for the originally dominant classes were drastically reduced. Nevertheless, the perturbed images are remarkably similar to the original ones. The main modifications mostly involved a slight decoloration of the target object in the various perturbed images. This fact is reflected in the difference images that are mostly black (i.e., zero values) but for a few colored pixels that sketch important features of the target objects. Notice, particularly, the cat image on the second row. In this case the perturbations focused on the cat’s features (e.g., its ears and tail) but also on a small cartoon on the upper right corner. It turns out that the cartoon contained a rough and undersampled sketch of a cat’s face which was also detected by the perturbation procedure. In the case of the sports car (4-th row in the figure) the main perturbation strategy seems to have been changing its color from bright red to a flatter orange hue. In all the image differences, important features (sometimes of specific colors) of the objects in question are highlighted from the black background.

The top 5 classes along with their associated VGG19 scores for the six image samples considered are shown in table 1 for the original and perturbed images in fig. 3. The sample number in table 1 corresponds to the row number (from the top to the bottom) in fig. 3. The relatively mild changes introduced into the original images resulted in drastic reductions of VGG19 scores for the originally dominant classes. The dominant classes for the perturbed images were in most cases qualitatively far from the original ones. An exception was sample 5 (“sport car”) which has a dominant perturbed class given by “amphibious vehicle” which is somewhat related to the original class. But even in this case the perturbed image contains practically the same object from the point of view of a human observer.

As mentioned in sec. 3, in addition to generating perturbations that minimize the top classes, it is also possible to attempt a maximization of a different class. For this, sample 1 was perturbed using eq. (2) and setting index m to the class corresponding to “polar bear”. The original dog image along with the resulting optimally perturbed one are shown in fig. 4. As for the samples shown above, here the perturbed image is very close to the original one while the VGG19 scores are also drastically different. It

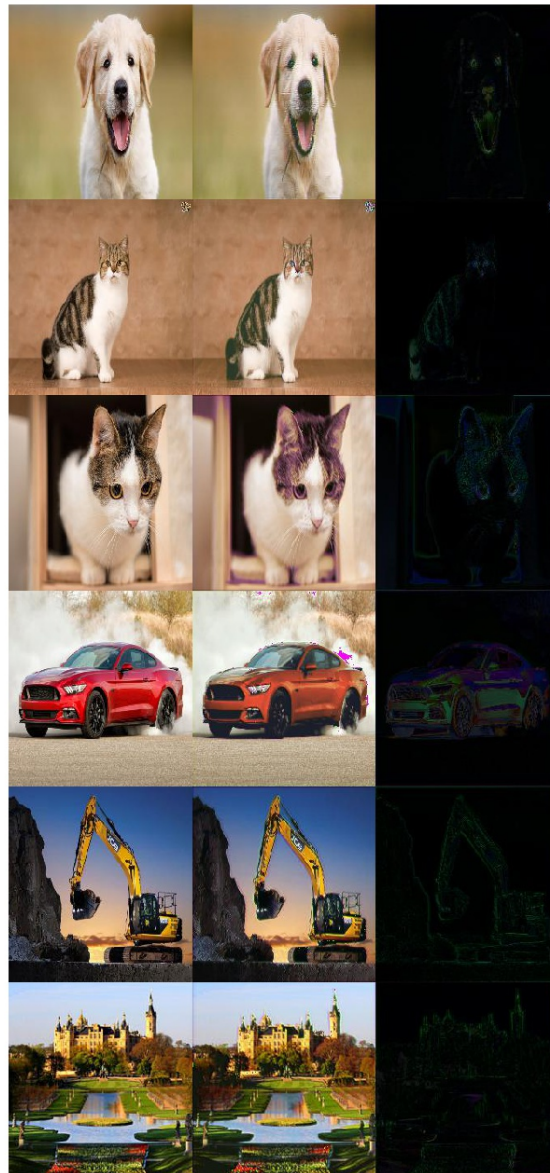


Figure 3: (Color online) Original sample images (first column) along with their corresponding optimally perturbed images (second column). The absolute value of the differences between original and perturbed images are shown on the third column. For all cases, the VGG19 scores corresponding to the dominant classes in the original images are drastically reduced in the perturbed ones. All the images available on github [47].

sample	original class	score	perturbed class	score
1	kuvasz	0.8234	African grey	0.9961
	Great Pyrenees	0.1412	muzzle	0.0007
	golden retriever	0.0236	kuvasz	0.0003
	Labrador retriever	0.0031	carriage dog	0.0003
	Old English sheepdog	0.0016	swab	0.0002
2	tabby cat	0.8022	king penguin	0.9877
	tiger cat	0.1246	prairie chicken	0.009
	Egyptian cat	0.0701	hare	0.0004
	Persian cat	0.0011	Egyptian cat	0.0004
	doormat	0.0004	albatross	0.0003
3	Egyptian cat	0.5098	screen	0.3684
	tabby cat	0.2082	monitor	0.3245
	tiger cat	0.0819	television	0.1768
	window screen	0.0631	computer keyboard	0.0433
	window shade	0.0317	notebook	0.0202
4	sport car	0.5307	amphibious vehicle	0.9783
	car wheel	0.1315	racing car	0.0067
	grille	0.1093	speedboat	0.0062
	convertible	0.1037	sport car	0.0026
	estate car	0.0631	car wheel	0.0023
5	crane	0.9656	mousetrap	0.2222
	wreck	0.0204	cassette	0.1466
	harvester	0.0024	iPod	0.0958
	container ship	0.0021	pencil sharpener	0.0585
	plow	0.0008	television	0.0562
6	castle	0.7823	desk	0.415
	lakeside	0.037	desktop computer	0.1414
	gondola	0.0344	monitor	0.0753
	submarine	0.029	screen	0.0506
	dock	0.0265	restaurant	0.0198

Table 1: Top 5 classes and associated VGG19 scores for the original and perturbed images for the six image samples considered.

is necessary to point out that, with the currently utilized perturbation generator, it was not possible to maximize every arbitrary class on a given image. Gradient descent runs on the same dog image that attempted to maximize the scores of “tabby cat” or “sea lion” did not converge.

4.3 Perturbing videos (I3D)

The video classification model I3D [44] was also analyzed by the perturbative procedure. Five video samples were randomly drawn from the kinetics video dataset [46]. A few frames extracted from each sample video are shown in fig. 5. The kinetics dataset extracts 10 seconds of video from publicly available YouTube samples. Each video is then assigned one of 400 categories corresponding to the predominant action in the sampled portion of the video. To perform the perturbative algorithm on the available GPU memory, the selected videos were undersampled by keeping only one of every 4 consecutive frames. I3D was able to correctly identify the assigned label in the undersampled videos. The top 5 original video classes along with their corresponding I3D scores are shown in table 2.

As was done for the case of images discussed above,



Figure 4: Original (a) and perturbed (b) images corresponding to a perturbation learned using eq. (2) that maximized the score for the “polar bear” class while attempting to keep the perturbed image as close as possible to the original one.

the video samples were perturbed following the algorithm in fig. 1. In this case the perturbation generator P consisted of blocks of 3D convolutional layers. The optimally perturbed videos successfully minimized the I3D scores for the top 5 original classes while keeping the perturbed video as close as possible to the original one. Frames from the perturbed videos are shown on the second rows (of each sample group) in fig. 5. Whereas the perturbed videos exhibit some blurred or decolored views, they still convey information about the originally labeled action from the point of view of a human observer. The third row (of each sample group) in fig. 5 shows frames from videos representing the (absolute value) differences between the original and perturbed videos. In general, the differences have near-zero pixel values everywhere but on pixels conveying important aspects of the main action being undertaken in the original video. The difference videos constitute sparse versions of the original videos that convey to a human observer the main points in the original videos.

The strategies followed by the perturbation algorithm in reducing the originally dominant class scores varied from sample to sample (see fig. 5). In sample 1 the perturbation strategy appears to have been a blurring of the images along with the removal of the red content in some of the frames. The red extracted content appears to come from the light shone on the coral and the scuba diver’s mask. The latter objects are informative of the main action that labels the original video (“scuba diving”, see table 2). The amount of introduced perturbations to the original frames in sample 1 is reduced by removing intensity from the red channels instead of the predominant green channels. The blurring in the perturbed sample 1 video may be attributed to mixing in the time dimension (i.e., mixing the pixels of adjacent

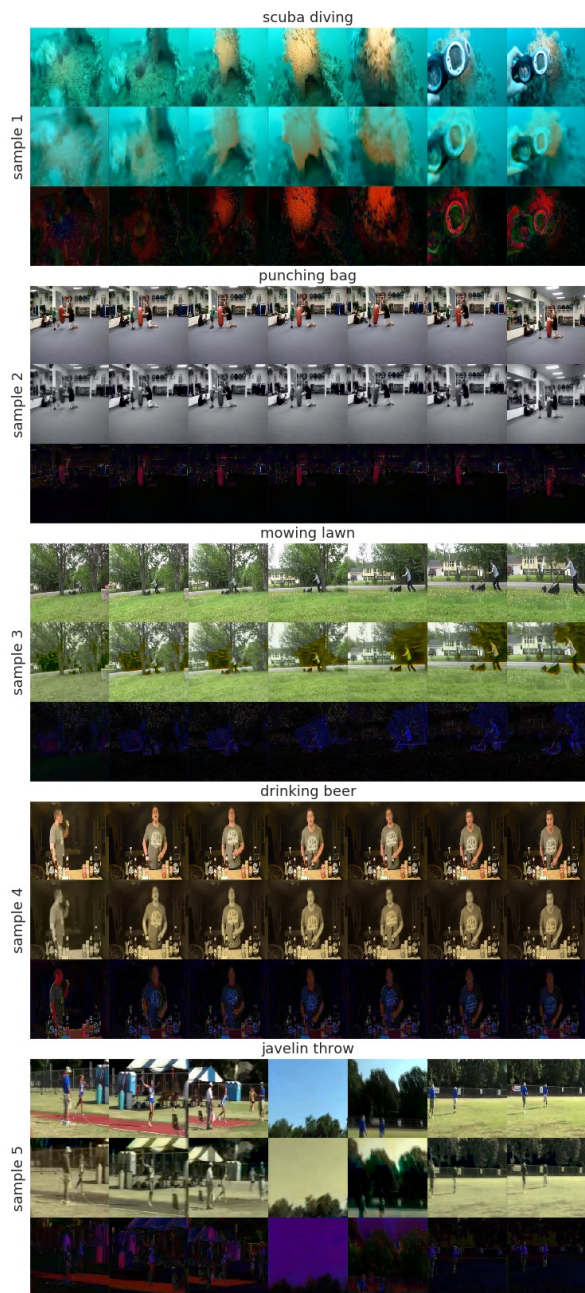


Figure 5: Video samples considered for perturbation analysis. The sample number and corresponding action (i.e., the class on the kinetics video dataset) are indicated on the right-hand side and top of each sample, respectively. For each sample seven frames from the original, perturbed, and difference videos are shown on the first, second and third row, respectively. All the videos are available on github [47].

frames). The perturbed video is classified as “smoking hookah”. While a human observer may not agree with such a classification of the perturbed video, the blurring in the video does make the frames images appear closer to containing smoke. The perturbations in sample 2 (“punching bag”) removed the red color from the punching bag which is then highlighted thorough the difference video. The perturbations also focused on the contours of certain objects and people in the video. The perturbed video for sample 2 is classified as “breakdancing”. Since punching bags are often red, the model may not have recognized the decolored bag and then observe the kicking child to classify the video as breakdancing. The perturbations in sample 3 (“mowing lawn”) do highlight a man pushing a lawn mower. By removing intensity from the blue channels (instead of the dominant green channels) modifications to the original image are reduced. A subtle perturbation to sample 3 appears to have been the blurring of the mowing man’s legs perhaps through targeted mixing in the time dimension. As a result the man is seen in the perturbed video slightly closer to being sliding. This may have influenced I3D’s classification of the perturbed sample 3 video as “toboganing”. For sample 4 there are three original dominant classes: “tasting beer”, “drinking beer” (the correct label in the kinetic dataset), and “bartending”. These three classes are of course related. Although the lighting in the original video is dark on the non-essential background, the perturbations further highlighted the important parts of the video, as can be seen in the difference video frames. The perturbed video is classified as “slacklining” (i.e., balancing on a tight rope) and “deadlifting” either of which would be challenging for a human observer to identify. Sample 5 was originally correctly classified as “javelin throw”. The perturbations leaved the images in the video largely decolored (particularly the originally bright blue sky). Although the essential aspects of the video are not modified from the point of view of a human observer, the perturbed video was classified by I3D as “ice skating”. By decoloring the images, the last frames of the video are slightly closer to presenting two people scating on an ice ring.

5 Discussion

5.1 Contrast to related perturbative techniques

Among the several previously published perturbative methods for analyzing deep learning models, the works by Fong and Vedaldi [11], Wei et. al. [25],

sample	original class	score	perturbed class	score
1	scuba diving	0.8832	smoking hookah	0.995
	snorkeling	0.114	smoking	0.004
	cleaning pool	0.0026	scuba diving	0.0008
	springboard diving	0.0002	swimming butterfly stroke	0.0001
	jumping into pool	0.0001	surfing water	0
2	punching bag	0.9183	breakdancing	0.9656
	drop kicking	0.0299	skateboarding	0.0143
	side kick	0.0226	jumpstyle dancing	0.0053
	punching person (boxing)	0.0048	krumping	0.0039
	exercising with an exercise ball	0.003	tap dancing	0.0023
3	mowing lawn	0.9681	tobogganing	0.9982
	walking the dog	0.0284	bobsledding	0.0006
	training dog	0.0034	training dog	0.0004
	sweeping floor	0	walking the dog	0.0004
	blowing leaves	0	mowing lawn	0.0003
4	tasting beer	0.449	slacklining	0.8925
	drinking beer	0.2442	deadlifting	0.0531
	bartending	0.2127	headbanging	0.0142
	opening bottle	0.0458	pull ups	0.0057
	drinking	0.0337	recording music	0.0023
5	javelin throw	0.9893	ice skating	0.9411
	long jump	0.0056	playing ice hockey	0.0188
	catching or throwing softball	0.0012	roller skating	0.0178
	throwing discus	0.0011	playing tennis	0.0053
	triple jump	0.0009	hockey stop	0.0046

Table 2: Top 5 classes and associated I3D scores for the original and perturbed images on the five video samples considered.

and Baluja and Fischer [18] share multiple similarities with the approach presented here. The versatility of our perturbation procedure allowed us to treat both image and video data. We are not aware of any previous perturbative procedure applied to both types of data.

In their image analysis, Fong and Vedaldi [11] learn a multiplicative mask for introducing blurring perturbations on an original image. The optimum perturbations then both localize the object in question and expose what the image classification model (VGG19) considered relevant in reaching its decision. Additionally, noise is also added to the images in order to avoid optimization artifacts. In our case the perturbations are not limited to blurring but can instead be more general. The convnets used here as perturbation generators are able to create nonlinearly perturbed images and videos by passing them through several stages of nonlinear transformations. This led to the production of efficiently targeted sparse perturbations allowing the resolution of details such as individual object features (see the differences images in fig. 3). Perhaps due to the sparsity of the introduced modifications to the inputs, we had no need for taking special precautions in order to avoid optimization artifacts.

Wei et. al. directly modify the pixels in video frames to iteratively reduce the original video’s dominant class score. The added perturbations are kept sparse by the addition of $L1$ - and $L2$ -norm loss terms

in the temporal and spatial dimensions, respectively. Additionally, a mask is also used to explicitly prevent modifications to some frames. In contrast, our video perturbations were generated by a convnet and can thus acquire a larger degree of nonlinearity customized to a particular sample. Moreover, we did not place any restrictions on what frames could be perturbed.

Baluja and Fischer [18] learned image perturbations that confuse target models by training convnets on datasets containing a number of image samples. In our case, perturbations are learned from a single image or video sample. This choice has consequences for the architectures used for generating the perturbations. Our perturbation generator P is intended to sequentially modify the input image or video while keeping its dimensions unmodified. Thus, all convolutional layers have a single input and a single output with the same dimensions as the input image or video. Essentially, a slightly modified version of the original image or video flows through the layers of P . This was considered important in keeping the perturbed image or video close to the input. Learning perturbations on a single sample has advantages and disadvantages. On the one hand, the perturbations learned by our method are specialized to the image or video in question. We are thus able to produce perturbations with rich detail on each sample, as shown above. On the other hand, having more data to learn perturbations from, Baluja and Fischer were able to create perturbations that forced target models to misclassify into arbitrarily chosen classes. Their approach is complementary to ours.

5.2 Object or action detection and explanation of model outcomes

The identification of portions of images or video frames that are found to be strongly correlated with the top scores of a classification model can be leveraged as a form of object or action detection [48, 49, 25]. In our case, the extracted sparse image or video differences (see figs. 3 and 5) indicate the locations of the most important features in the inputs. In contrast with other localization techniques [50, 51, 14, 52, 10, 48, 11], the highlighted features in the image or video differences are generally given here with a high level of detail and preserve the color information.

Another important aspect of the extracted perturbations is the insights they provide about what the models consider important in reaching a classification decision. Due to their increasing widespread application, machine learning models in general and deep

learning models in particular are required to show transparency in their decision process [24]. Additionally, understanding model outcomes is crucial for detecting and correcting possible errors or for enhancing model performance [9, 49]. The high resolution of the extracted perturbations shown above allow appreciating, in detail, what features the models have considered important. For instance, the eyes, nose, mouth, and even the red tongue of the dog in image sample 1 (top of fig. 3) are clearly delineated in the corresponding differences image. To different degrees, it is possible to understand the image and video perturbations in sec. 4 in intuitive terms. At the same time, the applied perturbations also exposed flaws in the studied models, as discussed next.

5.3 Enhancing model generalization through adversarial data augmentation

We discuss here an augmentation procedure similar to previously proposed schemes involving retraining on adversarial examples [12, 13, 20] but adapted to the perturbation method described in the present work. As discussed in sec. 5.2, the studied image and video classification models consider relevant features in reaching their decisions. On the other hand, slight perturbations can cause drastic misclassification (see figs. 3 and 5 and tables 1 and 2). The root of this problem may lie in the weight that the models assign to the various detected features. From a human’s point of view, the main features in the perturbed samples were still similar to the ones in the original images or videos. Moreover, any inserted features belonging to a different class in the perturbed samples were not important enough to change the sample class from a human’s perspective. This situation can be mitigated by “telling” the model about their misclassification through re-training [12, 13, 20]. The retraining would consist on a semi-supervised process. In this case, one would obtain an initial set of sparse perturbations (as done here for images and videos) for each sample in a training set and fine-tune the model with the correct labels (i.e., the original sample labels) for the perturbed samples. For fine-tuning purposes, the dataset does not have to be as large as the one used to originally train the model (e.g., such as the imagenet dataset [53] for VGG19), although it is indeed possible to retrain on the entire original dataset. Multiple perturbed instances for the same sample can be obtained by simply running several times the perturbation algorithm. It may also be possible to further augment the data by using other sparse perturbations [18, 25]. Once retrained, the

model can be re-evaluated through a new round of perturbations. At this point it is expected that less sparse perturbations will be needed in order to induce the retrained model to misclassify. The process can be repeated as many times as needed until the loss no longer converges under a threshold value during the perturbation procedure. For instance, the loss in our image and video experiments was generally reduced to values under 0.2, but in some situations (e.g., when attempting to change a dog image into a “sea lion”) the loss could not be made less than 1. Failure to drive down the loss in eq. (1) can be an indication that the class can not be modified without severely perturbing the original sample. Human supervision after each model retraining iteration is required for assessing whether or not perturbed samples still belong to the original class.

5.4 Image or Video compression and approximate reconstruction

The perturbations of images and videos in sec. (4) were found to be sparse but at the same time detailed in the features they represent (see the image or video differences in figs. (3) and (5)). We propose leveraging this concentrated form of information into a compression scheme. To obtain a compressed representation of an image or video first obtain a perturbed sample through the process described in sec. (3) and then calculate the difference $\delta^{(i)}$ between the original and perturbed samples,

$$\delta^{(i)} = \mathbf{X}^{(i)} - P^{(i)}(\mathbf{X}^{(i)}),$$

where i is a sample index, $\mathbf{X}^{(i)}$ is an image or video sample, and $P^{(i)}$ is a perturbation generator learned for $\mathbf{X}^{(i)}$. Most of the elements of array $\delta^{(i)}$ are expected to be approximately zero, as seen above. Thus, it is possible to obtain a sparse array from $\delta^{(i)}$ by thresholding its values. A more robust procedure for obtaining a sparse representation of $\delta^{(i)}$ is to apply to it a wavelet transform and threshold the result to obtain a set of sparse coefficients $\omega^{(i)}$, i.e.,

$$\omega^{(i)} = T \left(W \left(\delta^{(i)} \right) \right),$$

where W and T denote a wavelet transform and thresholding operators, respectively. The sparse coefficients $\omega^{(i)}$ contain only essential information about sample $\mathbf{X}^{(i)}$ from the point of view of the classification model M . Irrelevant contextual information is removed from $\omega^{(i)}$.

Approximate reconstruction could be achieved through training a neural network R as described

next. The sparse coefficients $\omega^{(i)}$ are first transformed to an image- or video-like array $\gamma^{(i)}$ through an inverse wavelet transform

$$\gamma^{(i)} = W^{-1}(\omega^{(i)}).$$

During training, the inputs of R are given by the set of sparse samples γ and its labels are the set of original samples \mathbf{X} . The optimum reconstruction model R is the result of the following minimization

$$\min_R (\mathbf{X} - R(\gamma)).$$

Model R 's architecture may consist of a set of deconvolutional layers [14] for upsampling the input sparse image (i.e., hence inducing the addition of context information to it) followed by convolutional and max-pooling layers for downsampling back to the original image or video dimensions. A trained model R can then be deployed for reconstructing approximate image or video samples $\chi^{(i)}$ from compressed coefficients $\omega^{(i)}$ by

$$\chi^{(i)} = R(W^{-1}(\omega^{(i)})).$$

Lacking exact contextual information, the reconstructed images or videos $\chi^{(i)}$ would likely be far from an accurate reconstruction of the original samples $\mathbf{X}^{(i)}$. The value of this scheme lies on the capability of transmitting a minimum compressed amount of relevant information given by the coefficients $\omega^{(i)}$. In the case of videos it may be advantageous to add a term to the loss for penalizing pixel value changes from frame to frame, effectively inducing the generation of a continuous background across frames. In some circumstances (e.g., the transmission of a movie under low-bandwidth conditions) it may be advantageous to overfit model R during training, effectively inducing R to “memorize” context information in the training set (a desirable situation assuming that only images or videos in the training set are to be transmitted).

6 Conclusions

We implemented a method for learning adversarial perturbations on images and videos with respect to their classification by deep convolutional network models. The sparse, but at the same time detailed, perturbations found allow a form of object or action recognition. The perturbations also provide insights into what features the models considered important when reaching their classification decisions. The sparse adversarial perturbations successfully confused the models into misclassifying while

still belonging to the original class from a human’s point of view. This may be leveraged for a proposed training procedure based on adversarial data augmentation. The sparsity and high detail of the learned perturbations may also be leveraged into a form of image or video compression and approximate reconstruction.

Acknowledgments

RRC acknowledges the support of the NSF (grant number CHE-1763198). HR acknowledges the support of the DOE (grant number DE-FG02-02ER15344). RRC also acknowledges the support of NVIDIA Corporation for the donation of the Titan X GPU used for this research.

References

- [1] Ben Goertzel and Cassio Pennachin. *Artificial general intelligence*, volume 2. Springer, 2007.
- [2] Alex Krizhevsky, Ilya Sutskever, and Geoffrey E Hinton. Imagenet classification with deep convolutional neural networks. In *Advances in neural information processing systems*, pages 1097–1105, 2012.
- [3] Karen Simonyan and Andrew Zisserman. Very deep convolutional networks for large-scale image recognition. *CoRR*, abs/1409.1556, 2014.
- [4] Kaiming He, Xiangyu Zhang, Shaoqing Ren, and Jian Sun. Deep residual learning for image recognition. In *Proceedings of the IEEE conference on computer vision and pattern recognition*, pages 770–778, 2016.
- [5] Kyunghyun Cho, Bart Van Merriënboer, Caglar Gulcehre, Dzmitry Bahdanau, Fethi Bougares, Holger Schwenk, and Yoshua Bengio. Learning phrase representations using rnn encoder-decoder for statistical machine translation. *arXiv preprint arXiv:1406.1078*, 2014.
- [6] Mariusz Bojarski, Davide Del Testa, Daniel Dworakowski, Bernhard Firner, Beat Flepp, Praseon Goyal, Lawrence D Jackel, Mathew Monfort, Urs Muller, Jiakai Zhang, et al. End to end learning for self-driving cars. *arXiv preprint arXiv:1604.07316*, 2016.
- [7] Angel Alfonso Cruz-Roa, John Edison Arevalo Ovalle, Anant Madabhushi, and Fabio Augusto González Osorio. A deep learning archi-

- ecture for image representation, visual interpretability and automated basal-cell carcinoma cancer detection. In *International Conference on Medical Image Computing and Computer-Assisted Intervention*, pages 403–410. Springer, 2013.
- [8] Yann LeCun, Yoshua Bengio, and Geoffrey Hinton. Deep learning. *nature*, 521(7553):436, 2015.
- [9] David Gunning. Explainable artificial intelligence (xai). *Defense Advanced Research Projects Agency (DARPA)*, *nd Web*, 2017.
- [10] Marco Tulio Ribeiro, Sameer Singh, and Carlos Guestrin. Why should i trust you?: Explaining the predictions of any classifier. In *Proceedings of the 22nd ACM SIGKDD international conference on knowledge discovery and data mining*, pages 1135–1144. ACM, 2016.
- [11] Ruth C Fong and Andrea Vedaldi. Interpretable explanations of black boxes by meaningful perturbation. *arXiv preprint arXiv:1704.03296*, 2017.
- [12] Christian Szegedy, Wojciech Zaremba, Ilya Sutskever, Joan Bruna, Dumitru Erhan, Ian Goodfellow, and Rob Fergus. Intriguing properties of neural networks. *arXiv preprint arXiv:1312.6199*, 2013.
- [13] Ian J Goodfellow, Jonathon Shlens, and Christian Szegedy. Explaining and harnessing adversarial examples (2014). *arXiv preprint arXiv:1412.6572*.
- [14] Matthew D Zeiler and Rob Fergus. Visualizing and understanding convolutional networks. In *European conference on computer vision*, pages 818–833. Springer, 2014.
- [15] Bolei Zhou, Aditya Khosla, Agata Lapedriza, Aude Oliva, and Antonio Torralba. Object detectors emerge in deep scene cnns. *arXiv preprint arXiv:1412.6856*, 2014.
- [16] Alexey Kurakin, Ian Goodfellow, and Samy Bengio. Adversarial examples in the physical world. *arXiv preprint arXiv:1607.02533*, 2016.
- [17] Yanpei Liu, Xinyun Chen, Chang Liu, and Dawn Song. Delving into transferable adversarial examples and black-box attacks. *arXiv preprint arXiv:1611.02770*, 2016.
- [18] Shumeet Baluja and Ian Fischer. Adversarial transformation networks: Learning to generate adversarial examples. *arXiv preprint arXiv:1703.09387*, 2017.
- [19] Seyed-Mohsen Moosavi-Dezfooli, Alhussein Fawzi, Omar Fawzi, and Pascal Frossard. Universal adversarial perturbations. *arXiv preprint*, 2017.
- [20] Aleksander Madry, Aleksandar Makelov, Ludwig Schmidt, Dimitris Tsipras, and Adrian Vladu. Towards deep learning models resistant to adversarial attacks. *arXiv preprint arXiv:1706.06083*, 2017.
- [21] Nicholas Carlini and David Wagner. Towards evaluating the robustness of neural networks. *arXiv preprint arXiv:1608.04644*, 2016.
- [22] Devansh Arpit, Stanisław Jastrzębski, Nicolas Ballas, David Krueger, Emmanuel Bengio, Maxinder S Kanwal, Tegan Maharaj, Asja Fischer, Aaron Courville, Yoshua Bengio, et al. A closer look at memorization in deep networks. *arXiv preprint arXiv:1706.05394*, 2017.
- [23] Chiyuan Zhang, Samy Bengio, Moritz Hardt, Benjamin Recht, and Oriol Vinyals. Understanding deep learning requires rethinking generalization. *arXiv preprint arXiv:1611.03530*, 2016.
- [24] Jan Philipp Albrecht. How the gdpr will change the world. *Eur. Data Prot. L. Rev.*, 2:287, 2016.
- [25] Xingxing Wei, Jun Zhu, and Hang Su. Sparse adversarial perturbations for videos. *arXiv preprint arXiv:1803.02536*, 2018.
- [26] Andrew G Howard. Some improvements on deep convolutional neural network based image classification. *arXiv preprint arXiv:1312.5402*, 2013.
- [27] Ren Wu, Shengen Yan, Yi Shan, Qingqing Dang, and Gang Sun. Deep image: Scaling up image recognition. *arXiv preprint arXiv:1501.02876*, 2015.
- [28] Antreas Antoniou, Amos Storkey, and Harrison Edwards. Data augmentation generative adversarial networks. *arXiv preprint arXiv:1711.04340*, 2017.
- [29] Francesco Calimeri, Aldo Marzullo, Claudio Stamile, and Giorgio Terracina. Biomedical data augmentation using generative adversarial neural networks. In *International Conference on Artificial Neural Networks*, pages 626–634. Springer, 2017.

- [30] Forest Agostinelli, Michael R Anderson, and Honglak Lee. Adaptive multi-column deep neural networks with application to robust image denoising. In *Advances in Neural Information Processing Systems*, pages 1493–1501, 2013.
- [31] Harold C Burger, Christian J Schuler, and Stefan Harmeling. Image denoising: Can plain neural networks compete with bm3d? In *Computer Vision and Pattern Recognition (CVPR), 2012 IEEE Conference on*, pages 2392–2399. IEEE, 2012.
- [32] Christian J Schuler, Harold Christopher Burger, Stefan Harmeling, and Bernhard Scholkopf. A machine learning approach for non-blind image deconvolution. In *Proceedings of the IEEE Conference on Computer Vision and Pattern Recognition*, pages 1067–1074, 2013.
- [33] Jian Sun, Wenfei Cao, Zongben Xu, and Jean Ponce. Learning a convolutional neural network for non-uniform motion blur removal. In *Proceedings of the IEEE Conference on Computer Vision and Pattern Recognition*, pages 769–777, 2015.
- [34] Pascal Vincent, Hugo Larochelle, Isabelle Lajoie, Yoshua Bengio, and Pierre-Antoine Manzagol. Stacked denoising autoencoders: Learning useful representations in a deep network with a local denoising criterion. *Journal of machine learning research*, 11(Dec):3371–3408, 2010.
- [35] Li Xu, Jimmy SJ Ren, Ce Liu, and Jiaya Jia. Deep convolutional neural network for image deconvolution. In *Advances in Neural Information Processing Systems*, pages 1790–1798, 2014.
- [36] Zhen Cui, Hong Chang, Shiguang Shan, Bineng Zhong, and Xilin Chen. Deep network cascade for image super-resolution. In *European Conference on Computer Vision*, pages 49–64. Springer, 2014.
- [37] Chao Dong, Chen Change Loy, Kaiming He, and Xiaoou Tang. Image super-resolution using deep convolutional networks. *IEEE transactions on pattern analysis and machine intelligence*, 38(2):295–307, 2016.
- [38] Yan Huang, Wei Wang, and Liang Wang. Bidirectional recurrent convolutional networks for multi-frame super-resolution. In *Advances in Neural Information Processing Systems*, pages 235–243, 2015.
- [39] Jian Wang, Mohit Gupta, and Aswin C Sankaranarayanan. Lisens-a scalable architecture for video compressive sensing. In *Computational Photography (ICCP), 2015 IEEE International Conference on*, pages 1–9. IEEE, 2015.
- [40] Michael Iliadis, Leonidas Spinoulas, and Aggelos K Katsaggelos. Deep fully-connected networks for video compressive sensing. *Digital Signal Processing*, 72:9–18, 2018.
- [41] Diederik P. Kingma and Jimmy Ba. Adam: A method for stochastic optimization. *CoRR*, abs/1412.6980, 2014.
- [42] Adam Paszke, Sam Gross, Soumith Chintala, Gregory Chanan, Edward Yang, Zachary DeVito, Zeming Lin, Alban Desmaison, Luca Antiga, and Adam Lerer. Automatic differentiation in pytorch. In *NIPS-W*, 2017.
- [43] Sébastien Marcel and Yann Rodriguez. Torchvision the machine-vision package of torch. In *Proceedings of the 18th ACM international conference on Multimedia*, pages 1485–1488. ACM, 2010.
- [44] Joao Carreira and Andrew Zisserman. Quo vadis, action recognition? a new model and the kinetics dataset. In *Computer Vision and Pattern Recognition (CVPR), 2017 IEEE Conference on*, pages 4724–4733. IEEE, 2017.
- [45] Yana Hassony. I3d models transfered from tensorflow to pytorch. https://github.com/hassony2/kinetics_i3d_pytorch, 2017.
- [46] Will Kay, Joao Carreira, Karen Simonyan, Brian Zhang, Chloe Hillier, Sudheendra Vijayanarasimhan, Fabio Viola, Tim Green, Trevor Back, Paul Natsev, et al. The kinetics human action video dataset. *arXiv preprint arXiv:1705.06950*, 2017.
- [47] Roberto Rey-de Castro. Adversarial perturbations on images and videos. <https://github.com/roberto1648/adversarial-perturbations-on-images-and-videos>, 2018.
- [48] Ramprasaath R Selvaraju, Michael Cogswell, Abhishek Das, Ramakrishna Vedantam, Devi Parikh, and Dhruv Batra. Grad-cam: Visual explanations from deep networks via gradient-based localization. In *ICCV*, pages 618–626, 2017.

- [49] Francois Chollet. *Deep learning with python*. Manning Publications Co., 2017.
- [50] Karen Simonyan, Andrea Vedaldi, and Andrew Zisserman. Deep inside convolutional networks: Visualising image classification models and saliency maps. *arXiv preprint arXiv:1312.6034*, 2013.
- [51] Jost Tobias Springenberg, Alexey Dosovitskiy, Thomas Brox, and Martin Riedmiller. Striving for simplicity: The all convolutional net. *arXiv preprint arXiv:1412.6806*, 2014.
- [52] Jianming Zhang, Zhe Lin, Jonathan Brandt, Xiao-hui Shen, and Stan Sclaroff. Top-down neural attention by excitation backprop. In *European Conference on Computer Vision*, pages 543–559. Springer, 2016.
- [53] Olga Russakovsky, Jia Deng, Hao Su, Jonathan Krause, Sanjeev Satheesh, Sean Ma, Zhiheng Huang, Andrej Karpathy, Aditya Khosla, Michael Bernstein, et al. Imagenet large scale visual recognition challenge. *International Journal of Computer Vision*, 115(3):211–252, 2015.